

# Efficient Crystal Structure Prediction Using Genetic Algorithm and Universal Neural Network Potential

Takuya Shibayama,<sup>1</sup> Hideaki Imamura,<sup>1</sup> Katsuhiko Nishimura,<sup>1</sup> Kohei Shinohara,<sup>1,\*</sup> Chikashi Shinagawa,<sup>1</sup> So Takamoto,<sup>1</sup> and Ju Li<sup>2</sup>

<sup>1</sup>*Preferred Networks, Inc., Tokyo 100-0004, Japan.*

<sup>2</sup>*Department of Nuclear Science and Engineering,  
and Department of Materials Science and Engineering,  
Massachusetts Institute of Technology, Cambridge, MA 02139, USA.*

(Dated: March 28, 2025)

Crystal structure prediction (CSP) is crucial for identifying stable crystal structures in given systems and is a prerequisite for computational atomistic simulations. Recent advances in neural network potentials (NNPs) have reduced the computational cost of CSP. However, searching for stable crystal structures across the entire composition space in multicomponent systems remains a significant challenge. Here, we propose a novel genetic algorithm (GA)-based CSP method using a universal NNP. Our GA-based methods are designed to efficiently expand convex hull volumes while preserving the diversity of crystal structures. This approach draws inspiration from the similarity between convex hull updates and Pareto front evolution in multi-objective optimization. Our evaluation shows that the present method outperforms the symmetry-aware random structure generation, achieving a larger convex hull with fewer trials. We demonstrated that our approach, combined with the developed universal NNP (PFP), can accurately reproduce and explore phase diagrams obtained through DFT calculations; this indicates the validity of PFP across a wide range of crystal structures and element combinations. This study, which integrates a universal NNP with a GA-based CSP method, highlights the promise of these methods in materials discovery.

## I. INTRODUCTION

Computational atomistic simulations based on a quantum-mechanical description enhances our understanding of materials and even contribute to modern materials design [1]. Crystal structure prediction (CSP), a process to predict stable crystal structures in given systems, is a crucial prerequisite to harness the computational atomic simulations [2–5]. Despite the well-established methodology for analyzing crystal structures from experimental data, CSP is essential for accelerating materials discovery through the ab initio approach.

While CSP plays an integral role in predicting stable crystal structures, it represents a daunting global optimization task owing to the vast energy landscape. Substituting elements from known crystal structure prototypes is a prevailing method for generating candidate structures [6]. Although the prototype substitution method often gives reasonable results, its coverage falls short, especially in multicomponent systems. Meta-heuristic algorithms offer another approach to creating novel crystal structures. These include methods such as random structure search [7], basin hopping [8], minima hopping [9, 10], genetic algorithm (GA) [11–15], particle swarm optimization [16], and Bayesian optimization [17, 18]. Typically, these CSP methods are combined with density functional theory (DFT) calculations to evaluate the formation energy of the candidate structures. However, the time-consuming DFT calculations,

which limit the exploration of structures, significantly hinder the efficiency of CSP.

Recent advancements in machine learning potential, interatomic potential fitted by DFT calculations, enable an efficient approach to CSP thanks to their fast and accurate energy evaluation [19–23]. Because we are often interested in multicomponent systems like ternary or quaternary systems in CSP, it is preferable for the machine learning potential to exhibit scalability with the number of elements and transferability across various systems. Also, high accuracy is required to capture subtle energy differences among distinct structures in CSP. A universal neural network potential (NNP) trained with extensive datasets has been gaining significant attention owing to its scalability and transferability, which includes M3GNet [24, 25], ALIGNN-FF [26], CHGNet [27], MACE-MP-0 [28, 29], GNoME [30], Orb [31], EquiformerV2-OMat24 [32, 33], MatterSim [34], and PFP [35–37].

Applying a universal NNP to CSP is straightforward. For example, GN-OA [38] combines the existing meta-heuristic algorithms with a universal NNP. GNoME [30] has unveiled various previously unreported stable structures with an extension of prototype substitution and random structure generation. Nevertheless, further development of CSP algorithms employing universal NNPs have room for enhancement. While the existing ab initio CSP methods often implicitly assume the number of energy evaluations to be limited due to the computational cost of DFT, the universal NNPs can allow us the vast number of energy evaluations and consider an entire convex hull concurrently, thereby appreciating the diversity of crystal structures all at once.

---

\* [kshinohara@preferred.jp](mailto:kshinohara@preferred.jp)

Here, we propose a novel CSP method using a universal NNP and GA. We have employed our developed universal NNP called PFP [36]. The current GA is inspired by the sophisticated multi-objective optimization algorithms [39, 40], which enables us to explore the entire composition space by exploiting the low-energy structure regions from optimization history. In this study, we use symmetry-aware random structure generation for the initial population and one of the mutation operations. Nevertheless, we mention that the present GA can be combined with other structure generation methods, such as generative models [41–43], which will be a future work.

The remainder of this paper is organized as follows. Section II describes PFP and a procedure for calculating formation energy with PFP in this study. Section III provides the details of the present GA for CSP. Section IV shows the application of the present GA to a chemically diverse range of elements, from binary to octonary systems.

## II. FORMATION ENERGY CALCULATION WITH PFP

### A. PFP

In this study, we used our developed universal NNP called the PFP version 6.0.0 [36], which was trained on around 42 million structures. The PFP can be applied to arbitrary combinations of 72 supported elements (all elements from H to Bi except Tc, Pm, Eu, Tb, Dy, Ho, Er, Tm, Yb, Lu, and Tl). Its training dataset was collected with DFT calculations using plane-wave basis sets and the projector augmented wave (PAW) [44, 45] with the Perdew–Burke–Ernzerhof (PBE) exchange-correlation functional [46] implemented in the Vienna ab-initio simulation package (VASP) [47–49]. Details of the DFT calculations are described in Ref. 36.

For systems containing V, Cr, Mn, Fe, Co, Ni, Cu, Mo, or W, we prepared the DFT calculations with the generalized gradient approximation (GGA) with PBE functional and GGA with Hubbard  $U$  corrections (GGA+ $U$ ) introduced by Dudarev et al. [50]. The  $U - J$  parameters in GGA+ $U$  were adopted from the Materials Project (MP) [51] except for Cu and from Wang et al. [52] for Cu. We trained PFP simultaneously for the DFT calculations with and without Hubbard  $U$  corrections. The PFP has two modes to predict energies with and without Hubbard  $U$  corrections. We used PFP trained with Hubbard  $U$  corrections for oxides and fluorides containing V, Cr, Mn, Fe, Co, Ni, Cu, Mo, or W, and otherwise without Hubbard  $U$  corrections. This choice is consistent with MP except for Cu.

### B. Reference simple systems

For formation energy calculations, we selected reference crystal structures for the 72 supported elements and 2 partially supported elements (Tc and Tl), as listed in Table I. For each element, we collected crystal structures from MP and searched for the lowest-energy structure after structural relaxation with PFP. The structural relaxation of atomic positions and lattice constants was performed until residual forces were less than  $5 \times 10^{-3}$  eV/Å. We matched the reference structures with the AFLOW standard encyclopedia of crystallographic prototypes [53] using `pymatgen` [54]. The third column of Table I displays the matched prototype structures within 0.1 meV/atom from the lowest-energy structure, which captures the diversity of stable prototype structures across various elements. The fourth column shows the PFP energy differences in meV/atom between two structures: one is the energy-lowest structure in PFP and the other is the energy-lowest structure in DFT calculation in MP. While the energy differences are particularly noticeable for layered or molecular crystal structures of B, O, As, and Br, possibly due to convergence issues in structural relaxations, PFP accurately evaluates stable crystal structures up to approximately 10 meV/atom.

### C. MP compatibility and energy corrections

Because we used almost the same DFT settings as MP, we applied anion and GGA/GGA+ $U$  mixing scheme corrections [55] into PFP total energies for better predictions across diverse chemical systems. The policy regarding which modes of PFP to use with and without Hubbard  $U$  corrections in Section II A is compatible with the GGA/GGA+ $U$  mixing scheme in MP. The exception is an oxide with Cu, in which case we use a correction for Cu in Ref. 56. Consequently, we can directly compare a convex hull with PFP and MP for all systems except oxides with Cu.

## III. GA-BASED CSP METHOD

In this study, we adopted a common terminology in the field of GA; each cycle for generating new structures from the previous ones is called a generation. A set of structures in a generation is called a population. Likewise, we refer to the process of generating a new structure and evaluating its formation energy as a trial. The present algorithm takes the following inputs: (i) elements (e.g., O–Sr–Ti), (ii) maximum number of atoms in the unit cell, (iii) population size, and (iv) number of total trials. Then, it outputs crystal structures on formation energy convex hulls based on PFP.

The workflow to search for stable crystal structures using GA is illustrated in Fig. 1. First, an initial population

TABLE I. Reference simple systems for each element in this study. The second column shows initial structures for structural relaxation taken from MP, recorded with `material_id`. The third column shows prototype structures within 0.1 meV/atom from the lowest-energy structure. When a prototype is not found, `material_id` is denoted instead. The fourth column shows the PFP energy differences (meV/atom) between the present reference structures and the on-the-hull structures in MP.

H	mp-973783	$\beta$ -O, mp-731827	4.3	Sr	mp-867202	A1 (fcc), A3 (hcp), A3' ( $\alpha$ -La), C19 ( $\alpha$ -Sm)	0.0
He	mp-614456	A1 (fcc), A3 (hcp)	0.8	Y	mp-112	A3 (hcp)	0.0
Li	mp-135	A2 (bcc)	0.7	Zr	mp-8635	A1 (fcc)	2.2
Be	mp-87	A3 (hcp)	0.0	Nb	mp-75	A2 (bcc)	0.0
B	mp-161	$\beta$ -B	40.5	Mo	mp-129	A2 (bcc)	0.0
C	mp-568286	mp-568286, mp-990424	0.6	Tc	mp-113	A3 (hcp)	0.0
N	mp-570747	$\gamma$ -N	5.7	Ru	mp-33	A3 (hcp)	0.0
O	mp-1180036	mp-1180036	41.3	Rh	mp-74	A1 (fcc)	0.0
F	mp-561203	A14 (molecular iodine)	0.0	Pd	mp-2	A1 (fcc)	0.0
Ne	mp-111	A1 (fcc)	0.0	Ag	mp-10597	A3 (hcp)	0.6
Na	mp-974920	A1 (fcc), A3 (hcp), A3' ( $\alpha$ -La), C19 ( $\alpha$ -Sm)	0.0	Cd	mp-94	A3 (hcp)	0.0
Mg	mp-1056702	A1 (fcc)	1.1	In	mp-973111	A3 (hcp)	1.9
Al	mp-134	A1 (fcc)	0.0	Sn	mp-117	A4 (diamond)	0.0
Si	mp-165	Lonsdaleite	5.9	Sb	mp-104	A7 ( $\alpha$ -As)	0.0
P	mp-1198724	mp-1198724	9.6	Te	mp-567313	A8 ( $\gamma$ -Se)	0.0
S	mp-666931	mp-666931	0.7	I	mp-23153	A14 (molecular iodine)	0.0
Cl	mp-1008394	A14 (molecular iodine)	0.0	Xe	mp-570510	A1 (fcc), A3 (hcp), A3' ( $\alpha$ -La), C19 ( $\alpha$ -Sm)	0.0
Ar	mp-568145	A1 (fcc), A3 (hcp)	0.0	Cs	mp-639727	A1 (fcc), A3 (hcp), A3' ( $\alpha$ -La)	0.0
K	mp-1184764	A1 (fcc), A3 (hcp), A3' ( $\alpha$ -La), C19 ( $\alpha$ -Sm)	0.0	Ba	mp-1096840	A2 (bcc)	0.0
Ca	mp-1183455	A1 (fcc), A3 (hcp), A3' ( $\alpha$ -La)	0.0	La	mp-156	A1 (fcc), A3' ( $\alpha$ -La)	0.0
Sc	mp-67	A3 (hcp)	0.0	Ce	mp-64	A20 ( $\alpha$ -U)	5.4
Ti	mp-46	A3 (hcp)	16.5	Pr	mp-38	A1 (fcc), A3 (hcp), A3' ( $\alpha$ -La), C19 ( $\alpha$ -Sm)	0.0
V	mp-146	A2 (bcc)	0.0	Nd	mp-123	A1 (fcc), A3' ( $\alpha$ -La), C19 ( $\alpha$ -Sm)	0.0
Cr	mp-90	A2 (bcc)	0.0	Sm	mp-21377	A1 (fcc), A3 (hcp), A3' ( $\alpha$ -La), C19 ( $\alpha$ -Sm)	0.0
Mn	mp-35	A12 ( $\alpha$ -Mn)	0.0	Gd	mp-155	A3 (hcp), C19 ( $\alpha$ -Sm)	0.0
Fe	mp-1271068	A2 (bcc)	0.0	Hf	mp-103	A3 (hcp)	0.0
Co	mp-54	A3 (hcp)	6.0	Ta	mp-50	A2 (bcc)	29.6
Ni	mp-23	A1 (fcc)	0.0	W	mp-91	A2 (bcc)	0.0
Cu	mp-30	A1 (fcc)	0.0	Re	mp-8	A3 (hcp)	23.6
Zn	mp-1187812	A3 (hcp), C19 ( $\alpha$ -Sm)	0.1	Os	mp-49	A3 (hcp)	0.0
Ga	mp-142	A11 ( $\alpha$ -Ga)	0.0	Ir	mp-101	A1 (fcc)	0.0
Ge	mp-1007760	Lonsdaleite	4.1	Pt	mp-126	A1 (fcc)	0.0
As	mp-11	A7 ( $\alpha$ -As)	23.0	Au	mp-1008634	A3 (hcp)	2.0
Se	mp-542605	mp-542605	1.1	Hg	mp-1184554	A3 (hcp), A3' ( $\alpha$ -La), C19 ( $\alpha$ -Sm)	2.4
Br	mp-1120813	mp-1120813	10.3	Tl	mp-151	A1 (fcc)	0.3
Kr	mp-976347	A1 (fcc), A3 (hcp), A3' ( $\alpha$ -La), C19 ( $\alpha$ -Sm)	0.0	Pb	mp-20745	A1 (fcc), A3 (hcp), A3' ( $\alpha$ -La)	0.1
Rb	mp-12628	A1 (fcc), A3 (hcp), A3' ( $\alpha$ -La), C19 ( $\alpha$ -Sm)	12.8	Bi	mp-23152	A7 ( $\alpha$ -As)	0.0

of structures is generated by random generation (Section III A). In each generation, structures are retrieved from the current population, and the promising ones are filtered (Section III B). Then, an elite population is generated and selected from the promising ones for crossover and mutation (Section III C). For the elite population, the next population is generated by crossover and mutation (Section III D). For the next population, the formation energy is calculated after structural relaxation with PFP, as described in Section II.

Note that we present the workflow in Fig. 1 with clarity, assuming a synchronous search is performed by each generation. However, an actual GA implementation can leverage asynchronous search over each trial, which en-

ables a high parallelism. When a structure is retrieved in a trial, its parent population is looked up from its generation. This asynchronous search can be performed effectively on top of the modern optimization framework *Optuna* [57].

### A. Random structure generation

To generate the initial population, we follow a random structure generation in Ref. 58. We split the cell into multiple sub-cells, randomly place atoms in only one of these sub-cells, and then replicated the sub-cell throughout the entire cell. This technique generates a diverse

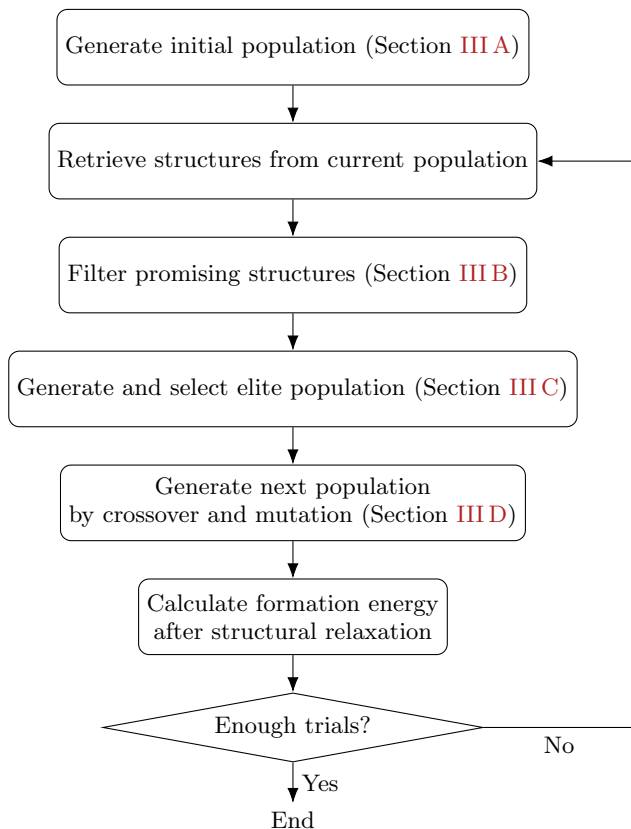


FIG. 1. Schematic diagram of the present GA-based CSP method.

set of structures, as opposed to randomly placing atoms in the entire cell which often generates randomly packed structures. We use symmetry-aware random structure generation by `PyXtal` [59] for the random structure generation in the sub-cells, thereby improving the search efficiency because stable crystal structures tend to have high symmetry [7].

The random structure generation by `PyXtal` requires a composition and a space-group type as input. We sampled the number of atoms in the unit cell uniformly up to the given maximum number of atoms in the unit cell and selected a composition from a multinomial distribution where each element has an equal probability. We sampled a space-group type uniformly from all space-group types other than  $P1$ . As some combinations of a composition and a space-group type are infeasible to generate a crystal structure, we retried the entire sampling process until a crystal structure is successfully generated.

## B. Population filtering

In this step, we selected structures close to the convex hull with the most recently updated composition. Our algorithm design is based on two intuitions: (1) lower-energy structures should exist near the structures close

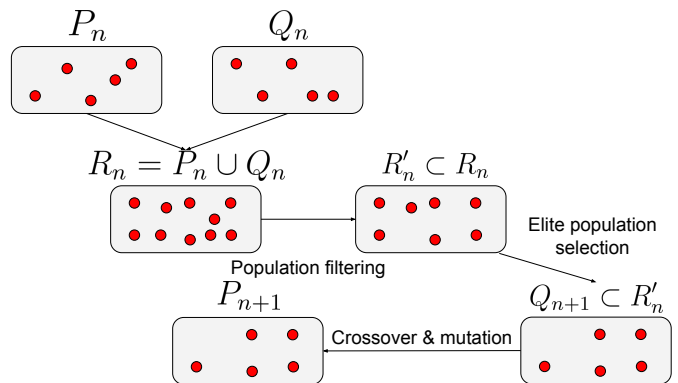


FIG. 2. The relationship between the parent population, elite population, filtered population, next elite population, and the next population.

to the convex hull, and (2) there should be some room for improvement in the neighbors of the compositions that observed recent updates on their lowest energy. Population filtering is similar to the aging evolution strategy [60] in that it ignores the structures that have not been updated for a long time.

Let  $M$  be the number of elements in the search,  $P_n$  be the parent generation,  $Q_n$  be the elite population used to select the parent generation, and  $R_n = P_n \cup Q_n$ , as shown in Fig. 2. Let  $E(i)$  be the energy of the structure  $i$ ,  $r(i) \in [0, 1]^M$  be the composition of the structure  $i$ , and  $j_*(i)$  be the structure with the smallest energy in the neighborhood of the structure  $i$  defined as follows:

$$j_*(i) = \operatorname{argmin}_{j \in \bigcup_{k=1}^n P_k} \{E(j) \mid \|r(i), r(j)\|_1 < \delta\}, \quad (1)$$

where  $\|x\|_1 = \sum_{k=1}^d |x_k|$  is the 1-norm, and  $\delta > 0$  is the threshold of the 1-norm of the composition. Here, we use all the structures we have explored so far  $\bigcup_{k=1}^n P_k$  as neighbors instead of  $R_n$  to maintain the diversity of the elite population. We define the distance to the convex hull of the structure  $i$  as

$$E(i) - E(j_*(i)). \quad (2)$$

Let  $n^*(i)$  be the generation in which the structure  $j_*(i)$  was generated. Let  $E_{\max}$  and  $E_{\min}$  be the maximum and minimum energies over all the structures explored so far defined as follows:

$$E_{\max} = \max\{E(i) \mid i \in \bigcup_{k=1}^n P_k\}, \quad (3)$$

$$E_{\min} = \min\{E(i) \mid i \in \bigcup_{k=1}^n P_k\}.$$

We later normalize the distance to the convex hull  $E(i) - E(j_*(i))$  to be between 0 and 1 by dividing it by  $E_{\max} - E_{\min}$ .

The population filtering is a procedure to construct a subset  $R'_n \subset R_n$ . For each element  $i$  in  $R_n$ , we calculated

the following quantity by considering the distance to the convex hull  $E(i) - E(j_*(i))$  and the generation difference  $n - n^*(i)$ ,

$$D(i) = \frac{E(i) - E(j_*(i))}{E_{\max} - E_{\min}} \times \alpha^{n - n^*(i)}, \quad (4)$$

where  $\alpha > 1$  is a tuning parameter. The parameter  $\alpha$  controls the importance of the generation difference. The smaller  $D(i)$  indicates that the structure is closer to the convex hull, and composition has been updated more recently. We adopt only the structures  $i$  that satisfy  $D(i) < \epsilon$ , where  $\epsilon$  is a tuning parameter. The parameter  $\epsilon$  controls the threshold of the distance to the convex hull and the generation difference. Finally, we define the following set  $R'_n$  as the output of this step,

$$R'_n = \{i \in R_n \mid D(i) < \epsilon\}. \quad (5)$$

### C. Elite population selection

The input of the elite population selection is the set  $R'_n$  of structures selected by the population filtering, and the output is the elite population  $Q_{n+1}$  to generate the next generation. The elite population is a set of structures to generate the next generation, and we select structures to apply crossover and mutation in the subsequent steps. We can reduce computational costs and search for stable structures more efficiently by applying crossover and mutation only to promising structures.

A commonly used method for selecting the elite population involves calculating the fitness of each structure and selecting the structures with the highest fitness [61–63]. For instance, ASE [61] defines it using the reciprocal of the energy of each structure. It only selects the structure with the highest fitness among the structures with the same composition. However, it does not use quantitative information about the composition and cannot maintain the diversity of the composition in the elite population.

Conversely, we selected the elite population using quantitative information about the composition in addition to the energy of the structure since the convex hull depends on both the energy and the composition. We found that the convex hull in the energy–composition space can be identified with the Pareto front in the multi-objective optimization problem (Fig. 3). The convex hull is designed to spread as much as possible downward in the energy axis direction, and the Pareto front is designed to spread as much as possible downward in the objective variable space.

We apply the elite population selection method used in the well-known genetic algorithms for multi-objective optimization problems, such as NSGA-II [39] and NSGA-III [40]. Notably, NSGA-II and NSGA-III are powerful algorithms for multi-objective optimization and are implemented in various black-box optimization software such

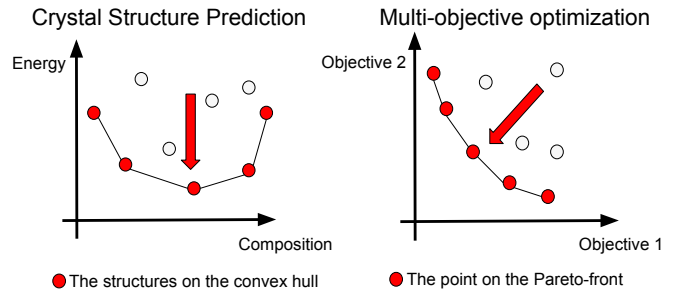


FIG. 3. The similarity between the convex hull in the energy–composition space and the Pareto front in the multi-objective optimization problem.

as Refs. [57] and [64]. The difference between NSGA-II and NSGA-III is the procedure for tie-breaking. In NSGA-II, a procedure is used to select structures with the smallest “crowding distance” for a set of structures of a certain rank. In NSGA-III, a procedure is used to draw a line called a “reference line” for a set of structures of a certain rank, calculate the crowding degree for each line, and select structures in order of less crowded. In general, NSGA-II is effective when the number of objective variables is 2–3, and NSGA-III is effective when it is 4 or more. The number of elements in the system is equal to the dimension of the multi-objective optimization in our problem.

Our proposed elite population selection method is summarized as follows. Note that we use the same notations as in Section III B.

1. Initialize the elite population  $Q_{n+1}$  as an empty set.
2. Sort the set  $R'_n$  by non-dominated sort with a partial order relation  $\prec$  that depends on both energy and composition, and assign a rank to each structure  $i \in R'_n$ .
3. Until the elite population  $Q_{n+1}$  exceeds the specified size, select structures in ascending order of rank and add them to the elite population  $Q_{n+1}$ .
4. When all structures of a certain rank  $k$  are added to the elite population  $Q_{n+1}$ , if the size of the elite population  $Q_{n+1}$  exceeds the specified size, select structures to add to the elite population  $Q_{n+1}$  from the structures of rank  $k$  according to a specific procedure.

Our proposed method is described in the following sections by defining the partial order  $\prec$  and the tie-breaking procedure for ranks. For later applications in Section IV, we use an NSGA-III-like tie-breaking procedure described in Section III C 3. We observed that the NSGA-III-like tie-breaking procedure outperformed the

NSGA-II-like one in our preliminary experiments, consistent with the general trend that NSGA-III is more effective in higher-dimensional optimization problems.

### 1. Partial order used for non-dominated sort

We formally define the energy–composition space as a subset of  $\mathbb{R}^{M+1}$ ,

$$\mathcal{R} = \left\{ (r_1, \dots, r_M, E) \in [0, 1]^M \times \mathbb{R} \mid \sum_{a=1}^M r_a = 1 \right\}. \quad (6)$$

For each  $a \in \{1, \dots, M\}$ , let  $r(i)_a$  be the ratio of the  $a$ -th element in the composition  $r(i)$ . We define the partial order  $\prec$  using the convex hull in the energy–composition space. Let  $H^0$  be the convex hull of the structures in  $R'_n$  in  $\mathcal{R}$ . Let  $H^1$  be the convex hull of the structures in  $R'_n \setminus H^0$ , and  $H^2$  be the convex hull of the structures in  $R'_n \setminus (H^0 \cup H^1)$ . Repeat this process, and let  $H^m$  be the convex hull of the structures in  $R'_n \setminus \left( \bigcup_{k=0}^{m-1} H^k \right)$ . By peeling off the thin skin from  $R'_n$  to obtain sets  $H^0, H^1, H^2, \dots$ , we define the partial order  $\prec$  like the relationship of  $i \prec j$  holds if and only if  $i \in H^k$  and  $j \in H^l$  where  $k < l$ . We can assign a rank to each structure by sorting  $R'_n$  using the partial order  $\prec$ . We denote the rank assigned to each structure  $i$  as  $k_i$ .

### 2. Tie-breaking procedure in NSGA-II-like CSP algorithm

First, we define a procedure using the crowding distance similar to NSGA-II. The definition of crowding distance is different because we consider a different problem from the usual multi-objective optimization problem.

Let  $H^{(k,a)}$  be the set of  $H^k$ , the output of the population filtering with rank  $k$ , sorted by  $r(i)_a$ . For each  $a \in \{1, \dots, M\}$  and structure  $i$ , let  $r(i)_{a,\text{left}}$  and  $r(i)_{a,\text{right}}$  be the ratio of the  $a$ -th element in the structures on both sides of  $i$  in  $H^{(k,a)}$ , and let  $\Delta_r(i, a)$  be the difference between them,

$$\Delta_r(i, a) = r(i)_{a,\text{right}} - r(i)_{a,\text{left}}. \quad (7)$$

Similarly, for the energy  $E(i)$ , let  $H^{(k,E)}$  be the set of  $H^k$  sorted by  $E(i)$ . For each structure  $i$ , let  $E(i)_{\text{right}}$  and  $E(i)_{\text{left}}$  be energies of the structures on both sides of  $i$  in  $H^{(k,E)}$  and  $\Delta_E(i)$  be the difference of them as follows:

$$\Delta_E(i) = E(i)_{\text{right}} - E(i)_{\text{left}}. \quad (8)$$

Note that the energy of each structure is min-max normalized for stability.

Using the  $\Delta_r(i, a)$  and  $\Delta_E(i)$  defined above, we define the crowding distance  $c(i)$  for the structures  $i$  in  $H^k$  as follows:

$$c(i) = \Delta_E(i) \times \sum_{a=1}^M \Delta_r(i, a). \quad (9)$$

We can order structures with the same rank by selecting structures with small crowding distance  $c(i)$ . The algorithm is summarized in Algorithm 1.

---

### Algorithm 1 Selection of $\ell$ Structures with Smallest Crowding Distance (NSGA-II Inspired)

---

**Require:** Population set  $H^k$  with rank  $k$ , number of selected structures  $\ell$

**Ensure:** Set  $\hat{H}^k$  containing  $\ell$  structures with smallest  $c(i)$

```

1: for each  $a \in \{1, \dots, M\}$  do
2:   Sort  $H^k$  by  $r(i)_a$  to create  $H^{(k,a)}$ 
3:   for each structure  $i \in H^k$  do
4:     Identify neighboring structures in  $H^{(k,a)}$ 
5:     Compute  $r(i)_{a,\text{left}}$  and  $r(i)_{a,\text{right}}$ 
6:     Compute  $\Delta_r(i, a) = r(i)_{a,\text{right}} - r(i)_{a,\text{left}}$ 
7:   end for
8: end for
9: Sort  $H^k$  by energy  $E(i)$  to create  $H^{(k,E)}$ 
10: for each structure  $i \in H^k$  do
11:   Identify neighboring structures in  $H^{(k,E)}$ 
12:   Compute  $E(i)_{\text{left}}$  and  $E(i)_{\text{right}}$ 
13:   Compute  $\Delta_E(i) = E(i)_{\text{right}} - E(i)_{\text{left}}$ 
14: end for
15: for each structure  $i \in H^k$  do
16:   Compute crowding distance:

```

$$c(i) = \Delta_E(i) \times \sum_{a=1}^M \Delta_r(i, a)$$

```

17: end for
18: Sort structures in  $H^k$  by  $c(i)$  in ascending order
19: Select the first  $\ell$  structures with the smallest  $c(i)$  to form  $\hat{H}^k$ 
20: return  $\hat{H}^k$ 

```

---

### 3. Tie-breaking procedure in NSGA-III-like CSP algorithm

Next, we define a procedure using a reference line similar to NSGA-III. The procedure for tie-breaking using the reference line in NSGA-III is performed as follows:

1. Normalize the value of each objective variable to be non-negative.
2. In the space of the objective variables, draw a line connecting the origin and the predetermined multiple reference points and construct multiple reference lines.
3. For each structure, project its objective variable values onto each reference line, select the reference line with the smallest distance to the projection point, and add it to the neighborhood set of each reference line.
4. Select the reference line with the smallest neighborhood set, select the structure closest to the reference line in the neighborhood set, and add this to the elite population by excluding it from the neighborhood set.

5. Repeat the above procedure until the elite population reaches the specified size.

To clarify the procedure, we need to define reference points and how to measure distances. We adopt the following distance:

$$d(i, j) = |E(i) - E(j)| \times \sum_{a=1}^M |r(i)_a - r(j)_a|. \quad (10)$$

We constructed the reference points as follows. For each composition axis  $a \in \{1, \dots, M\}$ , select the structure with the maximum  $r(i)_a$  in  $H^k$  and call them  $i_1, \dots, i_M$ . Then, consider an  $(M - 1)$ -dimensional simplex with  $i_1, \dots, i_M$  as vertices, and place points  $r_1, \dots, r_K$  uniformly at regular intervals on it, and use these as reference points. Here,  $K$  is determined by the number of points to be placed on the edge of the  $(M - 1)$ -dimensional simplex, and if  $k + 1$  points are placed on the edge,  $K = \binom{M+k-1}{k}$ . The algorithm is summarized in Algorithm 2.

---

**Algorithm 2** Selection of  $\ell$  Structures based on the Reference Line (NSGA-III Inspired)

---

**Require:** Population set  $H^k$  with rank  $k$ , number of selected structures  $\ell$

**Ensure:** Set  $\hat{H}^k$  containing  $\ell$  structures distributed along the reference lines

- 1: **Normalize** each objective variable to be non-negative
  - 2: **Construct reference lines:**
  - 3: Define  $K$  reference points by selecting structures  $i_1, \dots, i_M$  with maximum  $r(i)_a$  for each axis  $a \in \{1, \dots, M\}$
  - 4: Place  $K$  points  $r_1, \dots, r_K$  uniformly on an  $(M - 1)$ -dimensional simplex
  - 5: **for** each structure  $i \in H^k$  **do**
  - 6:     **for** each reference line  $j$  **do**
  - 7:         Project  $i$  onto reference line  $j$
  - 8:         Compute distance  $d(i, j) = |E(i) - E(j)| \times \sum_{a=1}^M |r(i)_a - r(j)_a|$
  - 9:     **end for**
  - 10:     Assign  $i$  to the reference line  $j^*$  with the smallest  $d(i, j)$
  - 11:     Add  $i$  to the neighborhood set of  $j^*$
  - 12: **end for**
  - 13: **while** size of  $\hat{H}^k$  is less than  $\ell$  **do**
  - 14:     Select reference line  $j^*$  with the smallest neighborhood set
  - 15:     Select structure  $i^*$  in the neighborhood set of  $j^*$  closest to the reference line
  - 16:     Add  $i^*$  to  $\hat{H}^k$  and remove it from the neighborhood set of  $j^*$
  - 17: **end while**
  - 18: **return**  $\hat{H}^k$
- 

#### D. Crossover and mutation

Crossover and mutation are the processes of generating new structures  $P_{n+1}$  from the elite population  $Q_{n+1}$ .

Crossover involves combining two parent structures to generate a child structure, and mutation involves changing the structure of a parent structure.

The crossover and mutations used in our proposed method are listed in Table II. Several methods are implemented in ASE [61], and others are our original methods. To customize the methods in ASE, we modify the implementation and release them as a package. [65]

The cut-and-splice crossover is a method to generate a child structure by cutting two parent structures at their unit cells along a crystal plane and joining them. Originally, its implementation in ASE only allowed crossover between parent structures with the same composition. We modify the implementation to allow crossover between parent structures with different compositions.

The random atom deletion mutation is a method to generate a child structure by randomly removing one atom from the parent structure. This mutation is effective to change the composition of the structure and explore the composition space.

The random structure generation mutation is a method to generate a child structure by the random structure generation in Section III A. This mutation can effectively maintain the diversity of the composition in the population.

## IV. RESULTS AND DISCUSSION

In this section, we present the results of our proposed method for CSP using PFP and GA. First, we evaluated the performance of the proposed method by comparing it with a random search in Section IV A. We then demonstrated the effectiveness of the proposed method by performing CSP searches for binary and ternary systems with MP in Section IV B. The results demonstrate that the proposed method can efficiently explore the search space and discover new crystal structure candidates that update the convex hull of MP. For the energy evaluation, we used the energy corrections described in Section II C.

### A. Quantitative comparison with random search and MP

We quantitatively evaluated the proposed method compared with a random search. The random search was performed using the method described in Section III A. In this experiment, we fixed the following inputs and parameters: the maximum number of atoms in the unit cell was 128, the population size was 250, the total number of trials was 50,000, and  $\alpha = 2.4$ ,  $\epsilon = 0.25$ . The genetic operations and their selection probabilities are listed in Table II. We chose four systems ranging from ternary to octonary systems: O–Sr–Ti and Ba–Ca–Cu–O–Ti as well known oxide systems [43], and Cu–Ga–Rh–Sc and Co–Cr–Cu–Fe–Mn–Ni–Ti–V as random alloy systems. The Hubbard  $U$  correction for Cu is applied for our method,

TABLE II. Crossover and mutation methods used in the proposed GA-based CSP method.

Method	Description	Implementation	Selection probability
Cut-and-splice crossover	Generate a child structure by cutting two parent structures at their unit cells along a crystal plane and joining them [62].	Modified ASE	1/2
Random composition mutation	Generate a child structure by randomly changing its composition.	ASE	1/12
Strain mutation	Distort the unit cell by applying a random strain matrix to the basis vectors.	ASE	1/12
Rattle mutation	Perturb the atomic positions by a random displacement.	ASE	1/12
Permutation mutation	Swap the atomic positions of two selected atoms.	ASE	1/12
Random atom deletion mutation	Generate a child structure by randomly removing one atom from the parent structure.	Original	1/12
Random structure generation mutation	Generate a structure by the random structure generation in Section III A.	Original	1/12

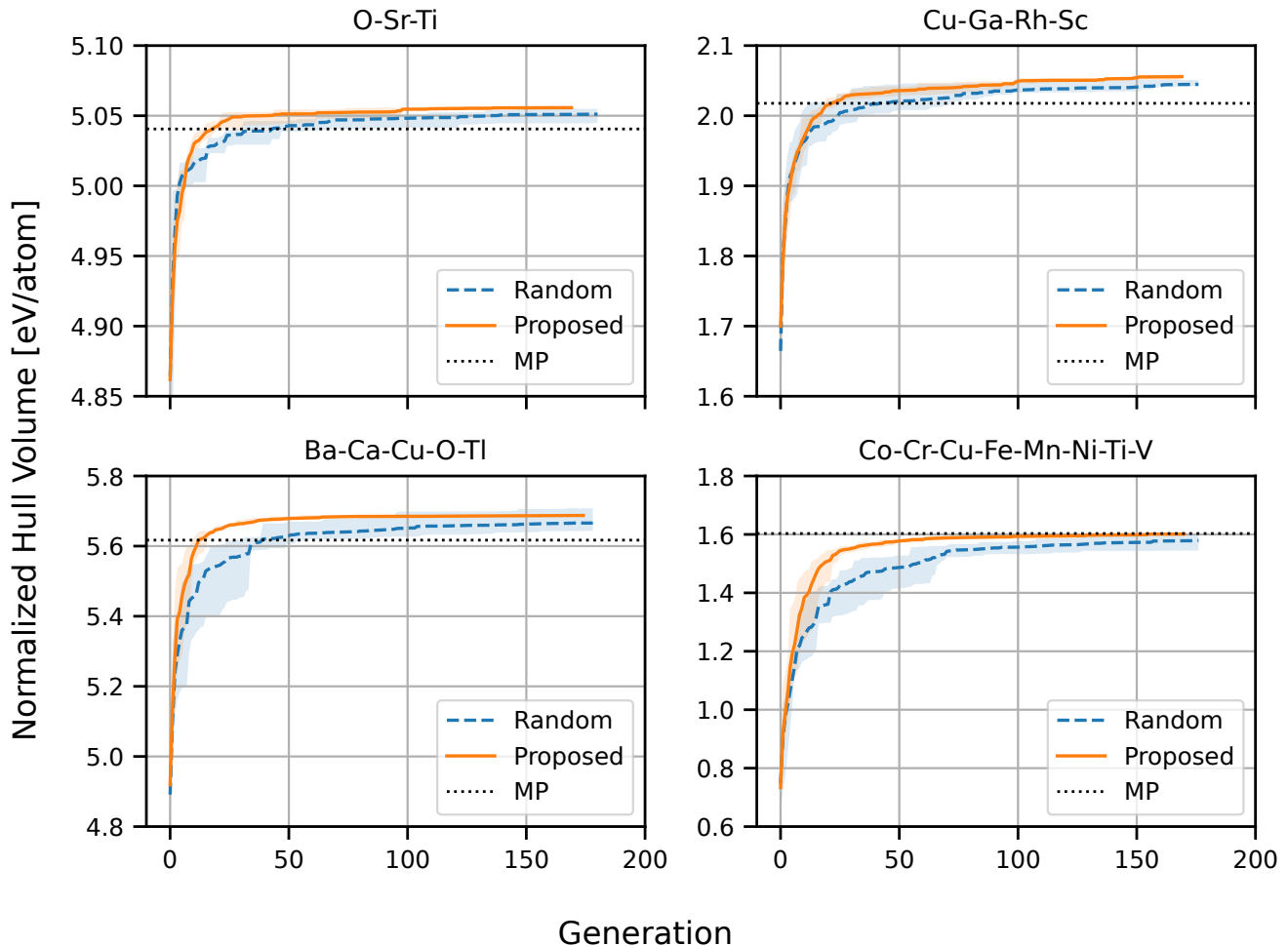


FIG. 4. Comparison between random search (orange) and the proposed method (blue) by the normalized hull volume history. The hatchings indicate the minimum and maximum normalized hull volumes within the five searches. The black dashed line indicates the normalized volumes for the convex hull constructed from MP structures.

while it is not applied for MP, which may affect the comparison in the Ba-Ca-Cu-O-Tl system, as mentioned in Section II A.

We evaluated each search by the volume of the convex hull, which can assess both the depth of the convex hull and the diversity of the included structures [66]. The

hull volume value of the  $M$ -element system is normalized by the unit hull volume  $V_{\text{unit},M} = 1 \text{ eV}/M!$ , which corresponds to the volume of the convex hull with only one crystal structure on the hull with formation energy of  $-1 \text{ eV/atom}$ . We performed the search by five times for each system because the CSP search involves ran-

domness. Additionally, we compared the normalized hull volume with that of MP. We performed structure optimization by PFP for MP structures within 0.2 eV/atom in MP convex hull to construct the MP convex hull. The absolute value of the normalized hull volume depends on the element system and cannot be compared across different systems.

Figure 4 illustrates how the normalized hull volume changed as the search progressed for each system, indicating that the proposed method outperformed random search for all the element systems. The final mean normalized hull volumes for each system are listed in Table III. Here, we denote the mean normalized hull volume as  $V_{\text{mean}}$ , the maximum as  $V_{\text{max}}$ , and the minimum as  $V_{\text{min}}$ . The improvements of final mean hull volumes of the proposed method compared with random search are 0.005, 0.011, 0.022, and 0.022 for O–Sr–Ti, Cu–Ga–Rh–Sc, Ba–Ca–Cu–O–Tl, and Co–Cr–Cu–Fe–Mn–Ni–Ti–V respectively. These improvements correspond to updates of the convex hull by 5 to 22 meV/atom if only one entry exists on the convex hull. We mention that the conversion of a normalized hull volume to a formation energy update depends on the shape of the convex hull. The updated hull volume by the proposed method compared with that of MP is 0.015, 0.038, 0.070, and -0.002 for O–Sr–Ti, Cu–Ga–Rh–Sc, Ba–Ca–Cu–O–Tl, and Co–Cr–Cu–Fe–Mn–Ni–Ti–V, respectively; this corresponds to 0.3, 1.9, 1.3, and -0.1% of MP hull volume, respectively. The proposed method achieved larger convex hull volumes than MP for systems except for the Co–Cr–Cu–Fe–Mn–Ni–Ti–V. In the five searches of the octonary alloy system, there are two crystal structures that are never found by proposed methods, as discussed later; this is attributed to the smaller convex hull volume compared to MP.

Figure 4 also depicts the efficiency of the CSP search with the proposed method. The number of generations required to reach 99% of each final hull volume for O–Sr–Ti, Cu–Ga–Rh–Sc, Ba–Ca–Cu–O–Tl, and Co–Cr–Cu–Fe–Mn–Ni–Ti–V were 7, 47, 16, and 61, respectively, for the proposed method, and 4, 66, 36, and 115, respectively, for a random search; this indicates that the proposed method can efficiently explore the search space, especially in multicomponent systems. Additionally, the figure exhibits that the proposed method has smaller fluctuations in the hull volume compared to random search. The fluctuation of the final hull volume for the five searches is calculated as  $(V_{\text{max}} - V_{\text{min}})/V_{\text{mean}}$ , which is 0.05, 0.35, 0.08, and 0.72% for the proposed method and 0.20, 0.44, 1.14, and 3.29% for random search for O–Sr–Ti, Cu–Ga–Rh–Sc, Ba–Ca–Cu–O–Tl, and Co–Cr–Cu–Fe–Mn–Ni–Ti–V, respectively; this indicates that the proposed method can stably explore the search space.

We validated the effectiveness of our proposed method for actual applications by comparing the convex hulls of CSP and that of MP. Table III shows the average number of MP structures below, around, and above the convex hull of CSP searches. The structures around the hull

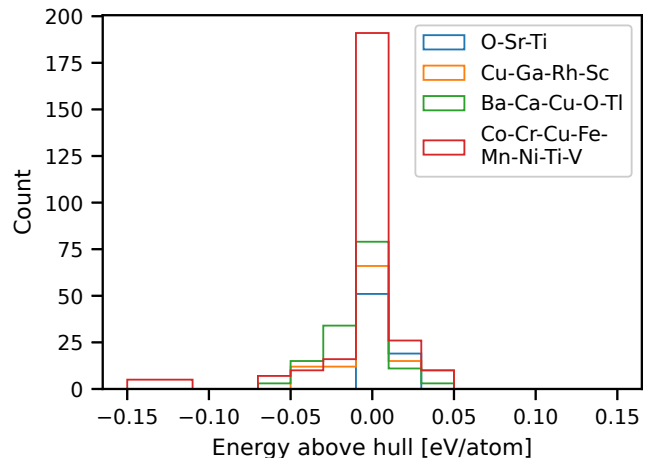


FIG. 5. Distribution of the energy above the hull of the crystal structures of MP. The convex hull is reconstructed using the CSP results obtained using the method proposed in Section IV A. The results of the five searches are aggregated and presented by the system.

are defined as those with energy above hull within 0.01 eV/atom. The structures below and above the hull are those with energy above hull less than -0.01 eV/atom and greater than 0.01 eV/atom, respectively. The average ratio of the number of MP structures around and above the convex hull to the total number of structures is 1.00, 0.79, 0.63, and 0.84 for O–Sr–Ti, Cu–Ga–Rh–Sc, Ba–Ca–Cu–O–Tl, and Co–Cr–Cu–Fe–Mn–Ni–Ti–V, respectively. Although the trends vary by element systems, around 80% of MP structures are reproduced by CSP. In particular, all MP structures are reproduced in the O–Sr–Ti system.

Figure 5 illustrates an energy above hull distribution of MP structures with the CSP hull by the proposed method. The results of the five searches are aggregated for each element system. As demonstrated, many MP structures are concentrated around the CSP hull. In this figure, MP structures with negative energy above hull indicate that the CSP search by the proposed method missed more stable structures in MP. For the octonary system of Co–Cr–Cu–Fe–Mn–Ni–Ti–V, two crystal structures shows energy above hull less than -0.1 eV/atom,  $\text{Cr}_2\text{Ti}$  (mp-1425) and  $\text{Mn}_2\text{Ti}$  (mp-1949). These structures are not found in all the five CSP searches, while random search was able to find  $\text{Cr}_2\text{Ti}$  twice and  $\text{Mn}_2\text{Ti}$  once in five searches in the potential energy landscape of PFP.

## B. CSP for binary and ternary systems

We demonstrated the capability of our CSP method using PFP to discover new crystal structure candidates for binary and ternary systems. The search conditions

TABLE III. Mean normalized hull volume and average number of MP hull structures compared with our CSP hull. The second columns show the mean normalized hull volume of the proposed method, while the last two columns show that for the random search and the normalized hull volume of MP, respectively. The third to fifth columns show the average number of MP structures below, around, and above the CSP hull by the proposed method, respectively (See the main text for the detailed definition). The sixth column shows the average ratio of the number of MP structures around or above the CSP hull.

System	$V_{\text{proposed}}$	Below hull	Around hull	Above hull	Reproducibility	$V_{\text{random}}$	$V_{\text{MP}}$
O–Sr–Ti	5.056	0	10.2	3.8	1.00	5.051	5.041
Cu–Ga–Rh–Sc	2.056	4.8	13.2	5	0.79	2.045	2.018
Ba–Ca–Cu–O–Tl	5.687	10.4	15.8	2.8	0.64	5.666	5.617
Co–Cr–Cu–Fe– Mn–Ni–Ti–V	1.601	8.6	38.2	7.2	0.84	1.579	1.603

were the same as those in Section IV A; however, the structures from MP are added to the initial population of the search. The crystal structures obtained from the search were re-evaluated using DFT calculations to verify their validity. We report the results for systems In–Li, As–V, Al–Li–Pd, and La–Mo–O shown in Figs. 6 and 7.

Figure 6 depicts the convex hulls by our CSP methods and MP, respectively. DFT calculations with VASP were performed for these structures using the same settings as in Section II A. By comparing convex hulls, the structures identified through our CSP method are confirmed to be also stable in DFT calculations. These findings suggest that the CSP approach using PFP is highly effective in discovering new crystal structure candidates.

Figure 7 shows comparisons of MP and CSP phase diagrams for ternary systems. Numerous promising new crystal candidates have also been discovered in the ternary systems. Our CSP methodology demonstrates the capability to explore and update the entire phase diagram comprehensively.

Crystal structures that update the convex hull of MP in the systems shown in Figs. 6 and 7 are listed in Table IV [67]. The space-group type was identified using `spglib` with `symprec = 0.01` and `angle_tolerance = 5` [68]. Additionally, we matched these crystal structures with AFLOW prototypes [53, 69–71] by assigning the AFLOW label using `aviary.wren` [72]. Several crystal structures were not found as prototype structures in the AFLOW database, indicating that our CSP method can discover novel crystal structures. Some of the listed crystal structures are visualized in Fig. 8.

## V. CONCLUSION

We have presented the efficient GA-based CSP method using our developed universal NNP, PFP. Our method comprehensively explores the entire composition space and successfully discovers numerous stable crystal struc-

tures. The proposed method even identified unregistered stable crystal structures in MP, and subsequent DFT calculations validated their stability. Given that CSP requires precise formation energy accuracy to distinguish various polymorphs, these results also demonstrate the validity of PFP for a wide range of crystal structures and element combinations. To efficiently search the entire composition space, we have proposed the novel elite population selection method inspired from multi-objective optimization techniques, which considers both formation energies and compositions. Since the proposed GA-based CSP method is agnostic to how to generate initial populations, it would be fruitful in future works to combine it with other structure generation methods to tackle the vast search spaces in CSP, such as generative models for crystal structures. Our present method and results show significant promise for accelerating materials discovery.

## ACKNOWLEDGMENTS

We would like to thank our colleagues from Preferred Networks, Inc. for helpful discussions and support, including Shuhei Watanabe. PFP v6 was developed using the National Institute of Advanced Industrial Science and Technology’s AI Bridging Cloud Infrastructure (ABCI) in addition to in-house supercomputers in Preferred Networks, Inc.

## COMPETING INTERESTS

T.S, H.I, K.N, K.S, C.S, and S.T are employees of Preferred Networks, Inc. Preferred Computational Chemistry Inc., a joint venture between Preferred Networks Inc. and ENEOS Corporation, offers a software-as-a-service called Matlantis, which incorporates a product based on this research.

[1] J. Hafner, *J. Comput. Chem.* **29**, 2044 (2008).

[2] A. R. Oganov, *Modern methods of crystal structure prediction* (John Wiley & Sons, 2011).

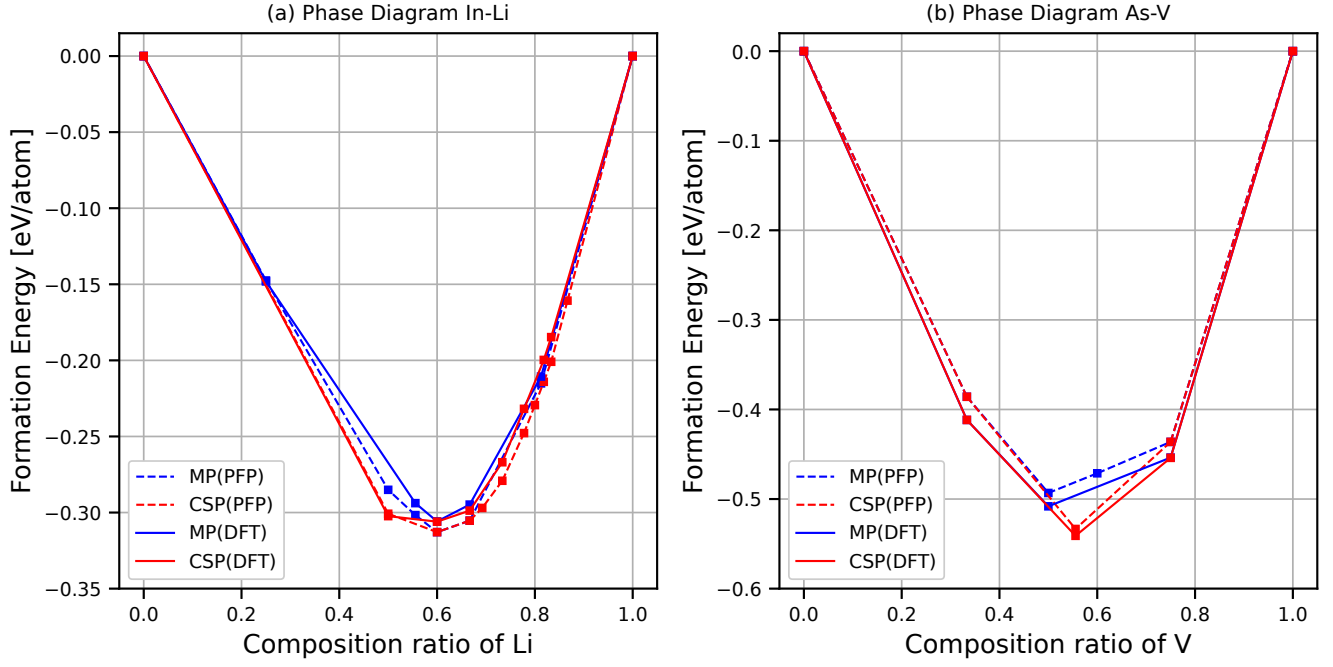


FIG. 6. Binary phase diagrams of (a) In–Li and (b) As–V systems. Red and blue lines show the convex hulls of the formation energy of our CSP results and MP, respectively. The energy is evaluated by VASP for solid lines, while PFP is used for dashed lines.

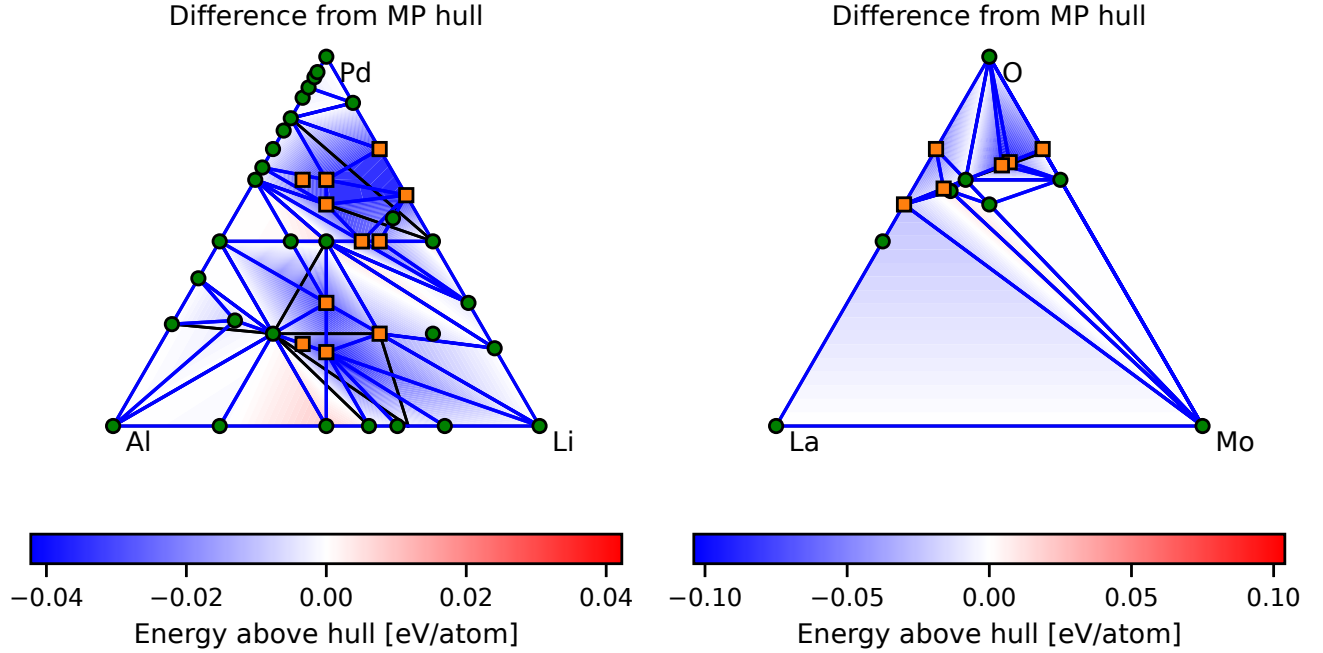


FIG. 7. Phase diagrams of ternary systems. Black and blue lines show the convex hulls of MP and our CSP results, respectively. Here, formation energies were evaluated with DFT calculations. Blue and red hatchings indicate the differences between the MP and our CSP convex hulls. The blue region shows the CSP results updating the MP convex hull. Markers display the simplices of the CSP convex hull, while orange squares indicate those with energy updates greater than 10 meV/atom.

[3] A. R. Oganov, C. J. Pickard, Q. Zhu, and R. J. Needs, *Nat. Rev. Mater.* **4**, 331 (2019).

[4] D. Wales, *Energy Landscapes: Applications to Clusters, Biomolecules and Glasses* (Cambridge University Press,

TABLE IV. List of crystal structures that update the convex hull. The fourth column shows the matched AFLOW prototype if it exists.

Formula	Space-group type	Hull energy update [meV/atom]	AFLOW prototype
In <sub>2</sub> Li <sub>2</sub>	<i>Pmma</i>	-35	AB_oP4_51_e_f-001
In <sub>2</sub> Li <sub>7</sub>	$P\bar{1}$	-1	
In <sub>4</sub> Li <sub>11</sub>	$P\bar{1}$	-10	
In <sub>4</sub> Li <sub>9</sub>	<i>C2/m</i>	-5	
As <sub>4</sub> V <sub>5</sub>	<i>I4/m</i>	-45	A4B5_tI18_87_h_ah-001
Al <sub>2</sub> Li <sub>2</sub> Pd	<i>C2/m</i>	-42	
Al <sub>2</sub> Li <sub>2</sub> Pd <sub>2</sub>	$P\bar{3}m1$	-34	
Al <sub>2</sub> Li <sub>2</sub> Pd <sub>6</sub>	$P2_1/m$	-33	
Al <sub>2</sub> Li <sub>4</sub> Pd <sub>2</sub>	$P4_2/mmc$	-14	
Al <sub>2</sub> Li <sub>4</sub> Pd <sub>6</sub>	$P2_1/m$	-25	
Al <sub>2</sub> Li <sub>6</sub> Pd <sub>8</sub>	$Im\bar{3}m$	-19	
Al <sub>2</sub> Li <sub>7</sub>	$P\bar{1}$	-4	
Al <sub>2</sub> LiPd <sub>6</sub>	$P\bar{1}$	-18	
Al <sub>3</sub> Pd <sub>7</sub>	<i>C2/m</i>	-4	
Al <sub>4</sub> Li <sub>3</sub> Pd <sub>2</sub>	$P\bar{3}m1$	-22	
Al <sub>4</sub> LiPd <sub>2</sub>	$P\bar{1}$	-8	
AlLi <sub>5</sub> Pd <sub>2</sub>	$P\bar{4}m2$	-4	
AlLiPd <sub>4</sub>	<i>Cmmm</i>	-33	
AlPd <sub>11</sub>	<i>Cmmm</i>	-3	
AlPd <sub>17</sub>	$P4/mmm$	-1	
Li <sub>33</sub> Pd <sub>55</sub>	$P\bar{1}$	-36	
LiPd <sub>3</sub>	<i>Cmmm</i>	-33	AB3_oC8_65_a_bf-001
La <sub>2</sub> O <sub>6</sub>	<i>C2/m</i>	-58	
La <sub>2</sub> Mo <sub>2</sub> O <sub>6</sub>	<i>R3c</i>	-1	
La <sub>2</sub> Mo <sub>4</sub> O <sub>15</sub>	$P\bar{1}$	-100	
La <sub>4</sub> Mo <sub>6</sub> O <sub>24</sub>	$P\bar{1}$	-105	
La <sub>4</sub> MoO <sub>9</sub>	<i>C2</i>	-12	
Mo <sub>3</sub> O <sub>9</sub>	<i>Cm</i>	-60	

- 2004).
- [5] A. Jain, Y. Shin, and K. A. Persson, *Nat. Rev. Mater.* **1**, 15004 (2016).
- [6] G. Hautier, C. Fischer, V. Ehrlicher, A. Jain, and G. Ceder, *Inorg. Chem.* **50**, 656 (2011).
- [7] C. J. Pickard and R. J. Needs, *J. Phys.: Condens. Matter.* **23**, 053201 (2011).
- [8] D. J. Wales and J. P. K. Doye, *J. Phys. Chem. A* **101**, 5111 (1997).
- [9] M. Amsler and S. Goedecker, *J. Chem. Phys.* **133**, 224104 (2010).
- [10] M. Krummenacher, M. Gubler, J. A. Finkler, H. Huber, M. Sommer-Jørgensen, and S. Goedecker, *SoftwareX* **25**, 101632 (2024).
- [11] D. M. Deaven and K. M. Ho, *Phys. Rev. Lett.* **75**, 288 (1995).
- [12] A. R. Oganov and C. W. Glass, *J. Chem. Phys.* **124**, 244704 (2006).
- [13] C. W. Glass, A. R. Oganov, and N. Hansen, *Comput. Phys. Commun.* **175**, 713 (2006).
- [14] D. C. Lonie and E. Zurek, *Comput. Phys. Commun.* **182**, 372 (2011).
- [15] Z. Falls, P. Avery, X. Wang, K. P. Hilleke, and E. Zurek, *J. Phys. Chem. C* **125**, 1601 (2021).
- [16] Y. Wang, J. Lv, L. Zhu, and Y. Ma, *Phys. Rev. B* **82**, 094116 (2010).
- [17] T. Yamashita, N. Sato, H. Kino, T. Miyake, K. Tsuda, and T. Oguchi, *Phys. Rev. Mater.* **2**, 013803 (2018).
- [18] M. K. Bisbo and B. Hammer, *Phys. Rev. Lett.* **124**, 086102 (2020).
- [19] J. Behler and M. Parrinello, *Phys. Rev. Lett.* **98**, 146401 (2007).
- [20] A. P. Bartók, M. C. Payne, R. Kondor, and G. Csányi, *Phys. Rev. Lett.* **104**, 136403 (2010).
- [21] A. V. Shapeev, *Multiscale Model. Simul.* **14**, 1153 (2016).
- [22] R. Drautz, *Phys. Rev. B* **99**, 014104 (2019).
- [23] E. V. Podryabinkin, E. V. Tikhonov, A. V. Shapeev, and A. R. Oganov, *Phys. Rev. B* **99**, 064114 (2019).
- [24] C. Chen, W. Ye, Y. Zuo, C. Zheng, and S. P. Ong, *Chem. Mat.* **31**, 3564 (2019).
- [25] C. Chen and S. P. Ong, *Nat. Comput. Sci.* **2**, 718 (2022).
- [26] K. Choudhary, B. DeCost, L. Major, K. Butler, J. Thiya-galingam, and F. Tavazza, *Digit. Discov.* **2**, 346 (2023).

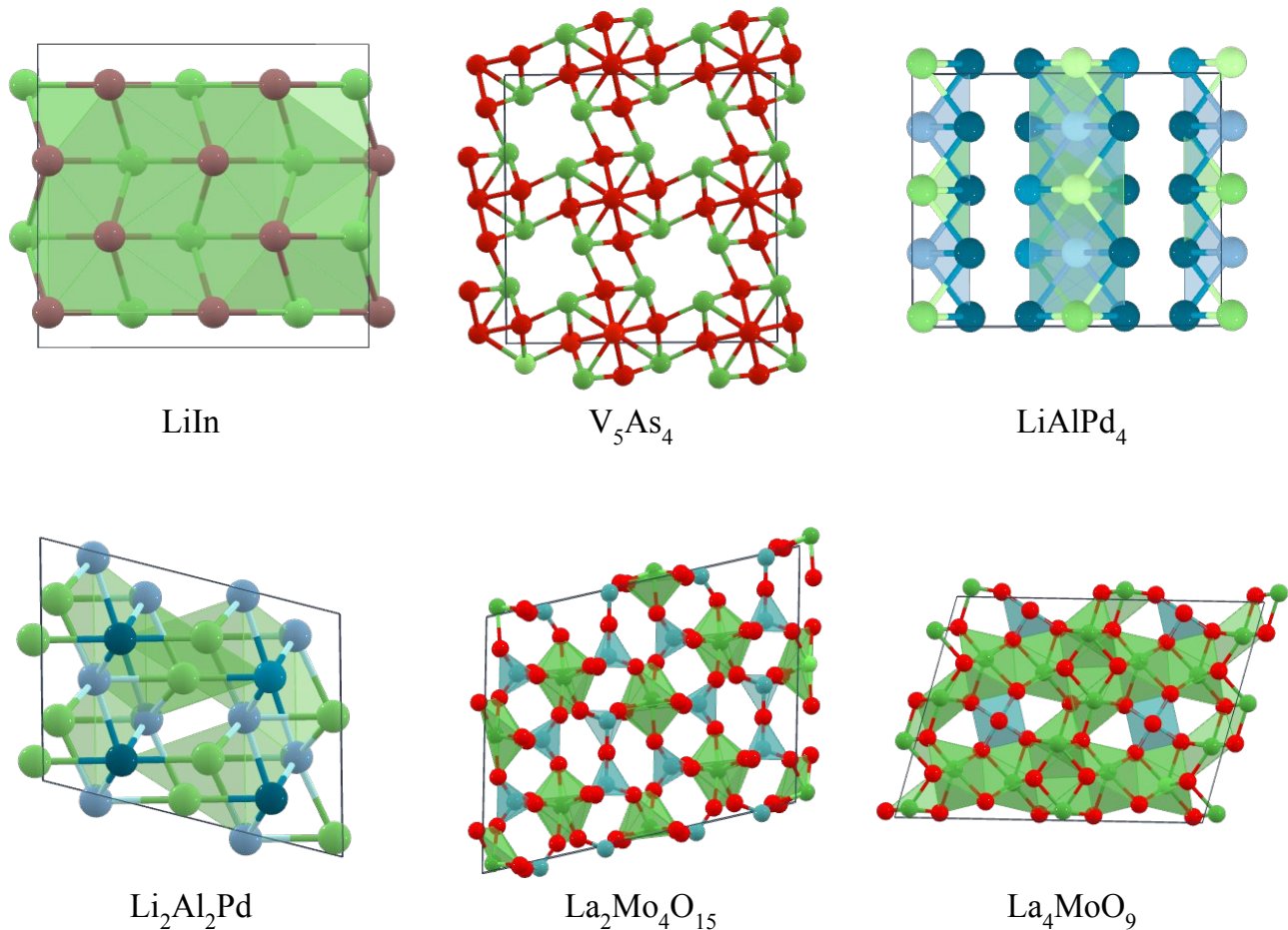


FIG. 8. Crystal structures that update the convex hull.

- [27] B. Deng, P. Zhong, K. Jun, J. Riebesell, K. Han, C. J. Bartel, and G. Ceder, *Nat. Mach. Intell.* **5**, 1031 (2023).
- [28] I. Batatia, D. P. Kovacs, G. Simm, C. Ortner, and G. Csányi, in *Advances in Neural Information Processing Systems*, Vol. 35, edited by S. Koyejo, S. Mohamed, A. Agarwal, D. Belgrave, K. Cho, and A. Oh (Curran Associates, Inc., 2022) pp. 11423–11436.
- [29] I. Batatia, P. Benner, Y. Chiang, A. M. Elena, D. P. Kovács, J. Riebesell, X. R. Advincula, M. Asta, W. J. Baldwin, N. Bernstein, A. Bhowmik, S. M. Blau, V. Cărare, J. P. Darby, S. De, F. D. Pia, V. L. Deringer, R. Elijošius, Z. El-Machachi, E. Fako, A. C. Ferrari, A. Genreith-Schriever, J. George, R. E. A. Goodall, C. P. Grey, S. Han, W. Handley, H. H. Heenen, K. Hermansson, C. Holm, J. Jaafar, S. Hofmann, K. S. Jakob, H. Jung, V. Kapil, A. D. Kaplan, N. Karimitari, N. Kroupa, J. Kullgren, M. C. Kuner, D. Kuryla, G. Liepuoniute, J. T. Margraf, I.-B. Magdău, A. Michaelides, J. H. Moore, A. A. Naik, S. P. Niblett, S. W. Norwood, N. O’Neill, C. Ortner, K. A. Persson, K. Reuter, A. S. Rosen, L. L. Schaaf, C. Schran, E. Sivonxay, T. K. Stenczel, V. Svahn, C. Sutton, C. van der Oord, E. Varga-Umbrich, T. Vegge, M. Vondrák, Y. Wang, W. C. Witt, F. Zills, and G. Csányi, “A foundation model for atomistic materials chemistry,” (2023), [arXiv:2401.00096](https://arxiv.org/abs/2401.00096).
- [30] A. Merchant, S. Batzner, S. S. Schoenholz, M. Aykol, G. Cheon, and E. D. Cubuk, *Nature* **624**, 80 (2023).
- [31] M. Neumann, J. Gin, B. Rhodes, S. Bennett, Z. Li, H. Choubisa, A. Hussey, and J. Godwin, “Orb: A fast, scalable neural network potential,” (2024), [arXiv:2410.22570](https://arxiv.org/abs/2410.22570).
- [32] L. Barroso-Luque, S. Muhammed, X. Fu, B. Wood, M. Dzamba, M. Gao, A. Rizvi, C. L. Zitnick, and Z. W. Ulissi, “Open materials 2024 (omat24) inorganic materials dataset and models,” (2024), [arXiv:2410.12771](https://arxiv.org/abs/2410.12771).
- [33] J. Schmidt, N. Hoffmann, H.-C. Wang, P. Borlido, P. J. Carriço, T. F. Cerqueira, S. Botti, and M. A. Marques, *Adv. Mater.* **35**, 2210788 (2023).
- [34] H. Yang, C. Hu, Y. Zhou, X. Liu, Y. Shi, J. Li, G. Li, Z. Chen, S. Chen, C. Zeni, M. Horton, R. Pinsler, A. Fowler, D. Zügner, T. Xie, J. Smith, L. Sun, Q. Wang, L. Kong, C. Liu, H. Hao, and Z. Lu, “Mattersim: A deep learning atomistic model across elements, temperatures and pressures,” (2024), [arXiv:2405.04967](https://arxiv.org/abs/2405.04967).

- [35] S. Takamoto, S. Izumi, and J. Li, *Comput. Mater. Sci.* **207**, 111280 (2022).
- [36] S. Takamoto, C. Shinagawa, D. Motoki, K. Nakago, W. Li, I. Kurata, T. Watanabe, Y. Yayama, H. Iriguchi, Y. Asano, T. Onodera, T. Ishii, T. Kudo, H. Ono, R. Sawada, R. Ishitani, M. Ong, T. Yamaguchi, T. Kataoka, A. Hayashi, N. Charoenphakdee, and T. Ibuka, *Nat. Commun.* **13**, 2991 (2022).
- [37] R. Jacobs, D. Morgan, S. Attarian, J. Meng, C. Shen, Z. Wu, C. Y. Xie, J. H. Yang, N. Artrith, B. Blaiszik, G. Ceder, K. Choudhary, G. Csanyi, E. D. Cubuk, B. Deng, R. Drautz, X. Fu, J. Godwin, V. Honavar, O. Isayev, A. Johansson, B. Kozinsky, S. Martiniani, S. P. Ong, I. Poltavsky, K. Schmidt, S. Takamoto, A. P. Thompson, J. Westermayr, and B. M. Wood, *Curr. Opin. Solid State Mater. Sci.* **35**, 101214 (2025).
- [38] G. Cheng, X.-G. Gong, and W.-J. Yin, *Nat. Commun.* **13**, 1492 (2022).
- [39] K. Deb, A. Pratap, S. Agarwal, and T. Meyarivan, *IEEE Trans. Evol. Comput.* **6**, 182 (2002).
- [40] K. Deb and H. Jain, *IEEE Trans. Evol. Comput.* **18**, 577 (2014).
- [41] T. Xie, X. Fu, O.-E. Ganea, R. Barzilay, and T. S. Jaakkola, in *ICLR* (2022).
- [42] R. Jiao, W. Huang, P. Lin, J. Han, P. Chen, Y. Lu, and Y. Liu, in *Workshop on "Machine Learning for Materials" ICLR 2023* (2023).
- [43] C. Zeni, R. Pinsler, D. Zügner, A. Fowler, M. Horton, X. Fu, Z. Wang, A. Shysheya, J. Crabbé, S. Ueda, R. Sordillo, L. Sun, J. Smith, B. Nguyen, H. Schulz, S. Lewis, C.-W. Huang, Z. Lu, Y. Zhou, H. Yang, H. Hao, J. Li, C. Yang, W. Li, R. Tomioka, and T. Xie, *Nature* (2025), 10.1038/s41586-025-08628-5.
- [44] P. E. Blöchl, *Phys. Rev. B* **50**, 17953 (1994).
- [45] G. Kresse and D. Joubert, *Phys. Rev. B* **59**, 1758 (1999).
- [46] J. P. Perdew, K. Burke, and M. Ernzerhof, *Phys. Rev. Lett.* **77**, 3865 (1996).
- [47] G. Kresse and J. Hafner, *Phys. Rev. B* **47**, 558 (1993).
- [48] G. Kresse and J. Furthmüller, *Phys. Rev. B* **54**, 11169 (1996).
- [49] G. Kresse and J. Furthmüller, *Comput. Mater. Sci.* **6**, 15 (1996).
- [50] S. L. Dudarev, G. A. Botton, S. Y. Savrasov, C. J. Humphreys, and A. P. Sutton, *Phys. Rev. B* **57**, 1505 (1998).
- [51] A. Jain, S. P. Ong, G. Hautier, W. Chen, W. D. Richards, S. Dacek, S. Cholia, D. Gunter, D. Skinner, G. Ceder, and K. A. Persson, *APL Mater.* **1**, 011002 (2013).
- [52] L. Wang, T. Maxisch, and G. Ceder, *Phys. Rev. B* **73**, 195107 (2006).
- [53] M. J. Mehl, D. Hicks, C. Toher, O. Levy, R. M. Hanson, G. Hart, and S. Curtarolo, *Comput. Mater. Sci.* **136**, S1 (2017).
- [54] S. P. Ong, W. D. Richards, A. Jain, G. Hautier, M. Kocher, S. Cholia, D. Gunter, V. L. Chevrier, K. A. Persson, and G. Ceder, *Comput. Mater. Sci.* **68**, 314 (2013).
- [55] A. Wang, R. Kingsbury, M. McDermott, M. Horton, A. Jain, S. P. Ong, S. Dwaraknath, and K. A. Persson, *Sci. Rep.* **11**, 15496 (2021).
- [56] A. Jain, G. Hautier, S. P. Ong, C. J. Moore, C. C. Fischer, K. A. Persson, and G. Ceder, *Phys. Rev. B* **84**, 045115 (2011).
- [57] T. Akiba, S. Sano, T. Yanase, T. Ohta, and M. Koyama, in *The 25th ACM SIGKDD International Conference on Knowledge Discovery & Data Mining* (2019) pp. 2623–2631.
- [58] A. O. Lyakhov, A. R. Oganov, and M. Valle, *Comput. Phys. Commun.* **181**, 1623 (2010).
- [59] S. Fredericks, K. Parrish, D. Sayre, and Q. Zhu, *Comput. Phys. Commun.* **261**, 107810 (2021).
- [60] E. Real, A. Aggarwal, Y. Huang, and Q. V. Le, in *Proceedings of the AAAI Conference on artificial intelligence*, Vol. 33 (2019) pp. 4780–4789.
- [61] A. H. Larsen, J. J. Mortensen, J. Blomqvist, I. E. Castelli, R. Christensen, M. Dułak, J. Friis, M. N. Groves, B. Hammer, C. Hargus, E. D. Hermes, P. C. Jennings, P. B. Jensen, J. Kermode, J. R. Kitchin, E. L. Kolsbjerg, J. Kubal, K. Kaasbjerg, S. Lysgaard, J. B. Maronsson, T. Maxson, T. Olsen, L. Pastewka, A. Peterson, C. Rostgaard, J. Schiøtz, O. Schütt, M. Strange, K. S. Thygesen, T. Vegge, L. Vilhelmsen, M. Walter, Z. Zeng, and K. W. Jacobsen, *J. Phys. Condens. Matter.* **29**, 273002 (2017).
- [62] L. B. Vilhelmsen and B. Hammer, *Phys. Rev. Lett.* **108**, 126101 (2012).
- [63] L. B. Vilhelmsen and B. Hammer, *J. Chem. Phys.* **141**, 044711 (2014).
- [64] J. Blank and K. Deb, *IEEE Access* **8**, 89497 (2020).
- [65] The modified crossover and mutation methods are available at <https://pypi.org/project/pfn-ase-extras/>.
- [66] S. Donaldson, R. A. Lawrence, and M. I. J. Probert (2024) [arXiv:2404.14354](https://arxiv.org/abs/2404.14354).
- [67] These crystal structures in xyz formats are available at Supplemental Materials.
- [68] A. Togo, K. Shinohara, and T. Isao, *Sci. Technol. Adv. Mater., Meth.* **4**, 2384822 (2024).
- [69] D. Hicks, M. J. Mehl, E. Gossett, C. Toher, O. Levy, R. M. Hanson, G. Hart, and S. Curtarolo, *Comput. Mater. Sc.* **161**, S1 (2019).
- [70] D. Hicks, M. J. Mehl, M. Esters, C. Oses, O. Levy, G. L. Hart, C. Toher, and S. Curtarolo, *Comput. Mater. Sci.* **199**, 110450 (2021).
- [71] H. Eckert, S. Divilov, M. J. Mehl, D. Hicks, A. C. Zettl, M. Esters, X. Campilongo, and S. Curtarolo, *Comput. Mater. Sci.* **240**, 112988 (2024).
- [72] R. E. Goodall, A. S. Parackal, F. A. Faber, R. Armiento, and A. A. Lee, *Sci. Adv.* **8**, eabn4117 (2022).